Subcooled Pool Boiling Experiments on Horizontal Heaters Coated With Carbon Nanotubes

V. Sathyamurthi
H-S. Ahn
D. Banerjee
S. C. Lau

Multiphase Flows and Heat Transfer Laboratory,
Department of Mechanical Engineering,
Texas A&M University,
College Station, TX 77843-3123

Pool boiling experiments were conducted with three horizontal, flat, silicon surfaces, two of which were coated with vertically aligned multiwalled carbon nanotubes (MWCNTs). The two wafers were coated with MWCNT of two different thicknesses: 9 μm (Type-A) and 25 μm (Type-B). Experiments were conducted for the nucleate boiling and film boiling regimes for saturated and subcooled conditions with liquid subcooling of 0–30°C using a dielectric fluorocarbon liquid (PF-5060) as test fluid. The pool boiling heat flux data obtained from the bare silicon test surface were used as a base line for all heat transfer comparisons. Type-B MWCNT coatings enhanced the critical heat flux (CHF) in saturated nucleate boiling by 58%. The heat flux at the Leidenfrost point was enhanced by a maximum of ~150% (i.e., 2.5 times) at 10°C subcooling. Type-A MWCNT enhanced the CHF in nucleate boiling by as much as 62%. Both Type-A MWCNT and bare silicon test surfaces showed similar heat transfer rates (within the bounds of experimental uncertainty) in film boiling. The Leidenfrost points on the boiling curve for Type-A MWCNT occurred at higher wall superheats. The percentage enhancements in the value of heat flux at the CHF condition decreased with an increase in liquid subcooling. However the enhancement in heat flux at the Leidenfrost points for the nanotube coated surfaces increased with liquid subcooling. Significantly higher bubble nucleation rates were observed for both nanotube coated surfaces. [DOI: 10.1115/1.3000595]

Keywords: pool boiling, critical heat flux, film boiling, nanotube, nanotechnology

1 Introduction

Boiling is the most efficient mode of heat transfer due to the inherent thermodynamics of the phase change phenomenon, which occurs reversibly at a constant temperature and at zero temperature gradient under uniform and infinitely slow heating. Hence, boiling is an attractive option for cooling of high heat flux devices. This work explores various potential transport mechanisms responsible for the enhancement of pool boiling heat fluxes on nanostructured surfaces using data obtained from subcooled and saturated pool boiling experiments.

Heater orientation, heater surface morphology, and thermophysical properties of the working fluid as well as the heater material, significantly alter transport mechanisms in pool boiling [1,2]. Enhancements in boiling heat transfer rates have been reported due to an increase in liquid subcooling and by employing various types of engineered microstructured surface morphologies (e.g., surface micromachined structures, graphite foams, and porous surfaces) [1,2]. Various studies reported the enhancement of pool boiling heat transfer by using newly developed materials or structures. Ramaswamy et al. [3,4] employed an enhanced structure composed of six layers of copper plates with rectangular channels machined into the substrates. This structure was used to investigate the combined effect of pressure and subcooling on the boiling performance of the enhanced structure. The authors reported that the combined effects of increasing subcooling and pressure enhanced the performance of boiling systems. They postulated that the increase in pore size and the reduction in pitch augmented the heat dissipation at wall superheats ranging from 4 K to12 K. Mudawar and Anderson [5] mounted a cylindrical pin-fin with microstructures machined into its perimeter onto an electronic chip. The critical heat flux (CHF) was enhanced in these experiments for liquid subcooling ranging from 0–35°C with FC-72 as the test fluid. Coursey et al. [6] applied graphite foams to thermal management of electronics. The foams had a porous structure consisting of interconnected graphite ligaments. The thermal conductivity of the foam was five times higher than copper. The authors claimed that the use of graphite foams as an evaporator in a thermosiphon enhanced the cooling of electronics, especially at lower chamber pressures.

Since the discovery of carbon nanotubes (CNTs) by Iijama [7] in 1991, there has been growing interest in the various applications of CNT. CNT have very broad ranges of thermal, electrical, and structural properties that may be tailored to various applications. According to Berber et al. [8], the thermal conductivity of CNT is 6600 W/m K, or about 16.5 times that of copper, at room temperature, but has a much lower value of 3000 W/m K, or about 7.6 times that of copper at 400 K. Ujereh and co-workers [9,10] reported results of their experiments on nucleate pool boiling of FC-72 on a silicon surface and on carbon nanotube coated surfaces under saturated conditions. The area of the heated surface was 12.7×12.7 mm^2. The multiwalled carbon nanotubes (MWCNTs) were synthesized using a calcined dendrimer catalyst in a plasma enhanced chemical vapor deposition (PECVD) system. The MWCNTs were 30 nm in diameter and 20–30 μm in length. The MWCNTs coated on a silicon wafer increased the CHF by 50% and enhanced the heat transfer coefficient by 400% compared with a bare silicon wafer. However, this study was restricted to nucleate boiling condition and the performance of the nanostructured surface over the film boiling regime was not reported. The authors noted that the synthesized MWCNTs did not

Contributed by the Heat Transfer Division of ASME for publication in the JOURNAL OF HEAT TRANSFER. Manuscript received November 28, 2007; final manuscript received September 9, 2008; published online April 30, 2009. Review conducted by Louis C. Burmeister. Paper presented at the 2007 ASME International Mechanical Engineering Congress (IMECE2007) Seattle, WA, November 10–16, 2007.

provide complete surface coverage. They reported no significant degradation of the MWCNT structures on the substrate as a result of the experiment.

This work is a continuation of a previous study where preliminary results for saturated pool boiling experiments on MWCNT coated heaters were reported [11]. The objective of this study was to investigate the effect of liquid subcooling on the pool boiling curve for MWCNT coated surfaces. In the present study, subcooled pool boiling experiments were performed on silicon wafers coated with MWCNTs of two different thicknesses of 9 μm and 25 μm, respectively. The boiling curves for the MWCNT coated wafers were compared with the boiling curve on an atomically smooth single crystal bare silicon wafer surface to identify the potential mechanisms responsible for heat flux enhancement (or lack of enhancement) on the MWCNT coated surfaces for the different boiling regimes.

2 Experimental Apparatus

The most significant component of the experimental apparatus was the boiling test surface. The boiling test surface consisted of one of the three silicon wafers. For each experiment, one of these wafers was fixed to the top of a copper cylinder. The surfaces of two of these silicon wafers were coated with MWCNTs of two different thicknesses: 9 μm (Type-A) and 25 μm (Type-B). The diagram of the experimental apparatus is shown in Fig. 1. Heat was supplied to the copper cylinder (diameter of 8.9 cm) from five embedded cartridge heaters. During the subcooled pool boiling experiments, the temperature of the test fluid was kept below its saturation temperature. Additional details of the experimental apparatus are also provided in Ref. [11].

A tubular heater was submerged in the test liquid. The tubular heater was used to raise and maintain the temperature of the test fluid at its saturation temperature ($\sim$56°C) in the saturated boiling experiments. For the subcooled boiling experiments, the temperature of the test fluid was kept below its saturation temperature with a coolant that was circulated from a constant temperature bath through a coiled copper heat exchanger placed just below the surface of the test fluid.

2.1 Test Surface Preparation and Characterization. For the pool boiling experiments in this study, two silicon wafers were coated with MWCNT using CVD. The MWCNT arrays had thicknesses of 9 μm and 25 μm. The details of the CVD process used in synthesis and growth of MWCNT forests were described in Ref. [12]. Vertically aligned MWCNT forests with a diameter of 8–15 nm were synthesized by passing 5 mol % C_2H_2 at 580 SCCM (SCCM denotes standard cubic centimeter per minute at STP) in helium at atmospheric pressure in a quartz tube furnace that was maintained at 680°C. A goniometer was used to measure the contact angle for PF-5060 on all the test surfaces. The contact angle for the bare surface was measured to be 10.5 deg, while for the Type-A and Type-B surfaces the contact angles were measured to be 9.6 deg and 13 deg, respectively. Thus, the test fluid PF-5060 wetted all the test surfaces very well. Contact angle measurements performed with water showed that the presence of nanotubes resulted in hydrophobic (Type-A $\sim$135 deg) and superhydrophobic (Type-B$\sim$153 deg) surfaces.

A recent study by Zhou et al. [13] showed the existence of wicking in "nanowicks" formed by mats of vertically aligned CNT on wafers. The study showed that the wicking of the liquid into the CNT mat occurred in three different flow topographies. They were: (a) corner flow (flow occurring between the edge of the CNT mat and the substrate), (b) top surface flow (flow on the CNT tips due asperities), and (c) interstitial flow (flow through the interstitial spaces between the dense CNT mats). According to this study, the surface flow was faster but less persistent than interstitial flow. Thus a liquid droplet first spread on the surface the CNT mats creating air-pockets. Subsequently, interstitial flow gradually reduced the air-pockets. The reports in the literature show that

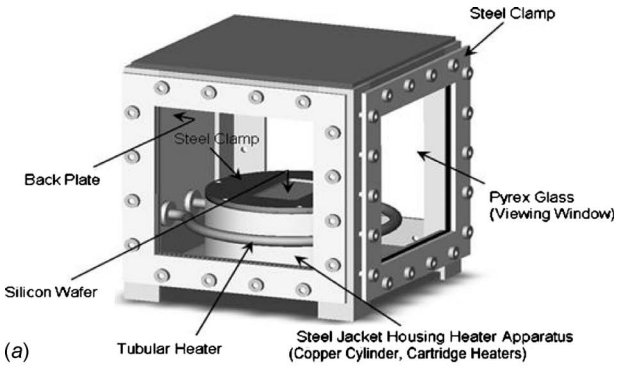

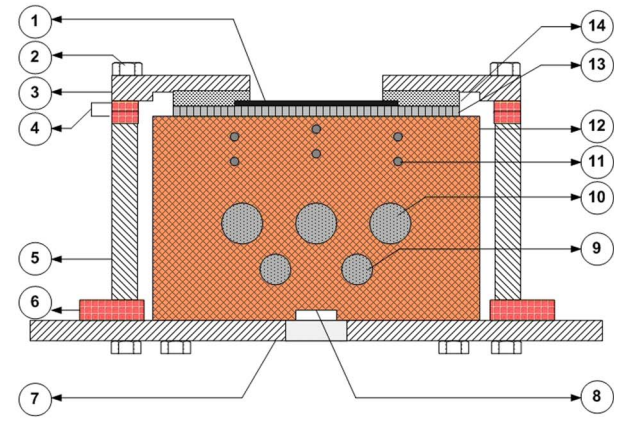

1. Test surface
2. M-4 nut
3. Steel clamp
4. Silicone rubber gaskets (1/16")
5. Steel jacket
6. Silicone rubber gasket (1/8")
7. Bottom cover plate with hole for lead wires
8. Groove for lead wires
9. 300W cartridge heater
10. 500W cartridge heater
11. K-type thermocouple
12. Copper cylinder
13. Pyrex glass wafer
14. Teflon gasket

(b)

Fig. 1 Design of experimental apparatus: (*a*) test section in viewing chamber, (*b*) schematic of the heater apparatus [11,15]

PF-5060 has a high solubility for air (50–60% by volume) [14]. Thus it is reasonable to expect that most air-pockets are eliminated when the CNT coated silicon wafers are submerged in the pool of PF-5060.

2.2 Test Section. Five cartridge heaters were inserted horizontally near the bottom of the copper cylinder, as shown in Fig. 1(*c*). A Pyrex® wafer was sandwiched between the silicon wafer and the top of the copper cylinder to minimize the electrical noise from the heaters. High thermal conductivity grease was used to minimize thermal contact resistance between surfaces at the various interfaces. Twelve K-type thermocouples were used to determine the temperature distribution in the copper cylinder. The junctions of these thermocouples were installed inside the copper cylinder at different vertical and radial positions such that they were aligned vertically. Additional thermocouples were placed in the test fluid PF-5060 to monitor the bulk temperature and the uniformity of the bulk liquid temperature. The transient signals from the thermocouples were digitized and recorded using an automated computer-controlled data acquisition system. A concentric annular stainless steel jacket with an inside diameter of 9.9 cm and a thickness of 7.6 mm was placed concentrically with the copper cylinder. The stainless steel jacket was separated from the copper cylinder by an air gap, which served as an insulation to minimize heat losses from the sides. A guard heater placed con-

centric with the steel jacket was used in the saturation experiments to maintain the bulk liquid at saturation temperature in the low heat flux regime. The silicon wafer was mounted on top of the copper cylinder and covered with an annular steel clamp fitted with a Teflon gasket (Fig. 1) to prevent any leaks. The steel clamp was seated on silicone rubber gaskets placed on top of the stainless steel jacket using M-4 nuts. Silicone rubber gaskets were also placed under the steel jacket and steel clamp to prevent leaks. The area of the test surface (silicon wafer with or without MWCNT coating) that was exposed to the test fluid during pool boiling was measured to be 5.9×3.2 cm^2 with chamfer radius of 0.3 cm.

2.3 Heat Exchanger for Subcooled Boiling Experiments. During the subcooled boiling experiments, the test fluid was maintained at a liquid subcooling of 5°C, 10°C, 20°C, or 30°C. The liquid was subcooled using a coiled copper heat exchanger. The heat exchanger coil was submerged 1.5 cm below the surface of the test fluid. The coolant within the heat exchanger was circulated using an external constant temperature bath with an electronic controller (Fig. 1(*b*)). The flow rate and the temperature of the coolant were adjusted and monitored to achieve the desired subcooling of the test fluid. During the saturated boiling experiments, the coiled copper tube heat exchanger was lifted above the surface of the test fluid.

3 Experimental Procedure

Prior to performing an experiment, one of the three test wafers was clamped on top of the copper cylinder. The viewing chamber was filled with PF-5060. The tubular heater was used to boil the test fluid for approximately 30 min at atmospheric pressure, for degassing purposes prior to each test. The power supplied to the tubular heater during degassing was ~300–500 W. It has been shown by Bhavnani et al. [14] that the percentage of dissolved air in PF-5060 does not decrease below 39% even after several days of degassing under atmospheric conditions. Hence, it is expected that the working liquid was not completely degassed under subcooled conditions since the test chamber was maintained at atmospheric pressure. The dissolved air content was not measured in this study. It can be expected however that the dissolved air content remained approximately the same after the degassing procedure prior to each run at saturated or subcooled conditions due to the fixed duration of degassing. Furthermore, completely degassed perfluorocarbon fluids are not encountered in practical phase change cooling applications. The noncondensable gases and vapor released during degassing was allowed to escape through the vent pipe, located at the back of the test section.

Some of the test fluid vapors that passed through the vent pipe during the degassing was recovered in the collection bottle by condensation for reuse. After the degassing step, the input power to the tubular heater was then adjusted to maintain the test fluid at its saturation temperature for the saturated pool boiling experiments. For a subcooled boiling experiment, the heat exchanger coil was lowered into the liquid pool prior to degassing.

The power input to the cartridge heaters was ramped in steps of 3–5 V for each data point on the boiling curve. Once steady state conditions were reached, the temperatures in the copper cylinder were recorded with the computer-controlled data acquisition system. The liquid pool temperature and ambient air temperature were also monitored with wire-bead thermocouples. The voltage and current supplied to the cartridge heaters were measured with a digital TRMS voltmeter and a digital TRMS clamp ammeter, respectively, at each steady state condition. After the CHF condition was achieved, the voltage input was increased slightly to cause transition to film boiling. To prevent burnout, the power supplied to the cartridge heaters was decreased quickly once a stably stratified vapor film covered the test surface. The system was then allowed to attain steady state. The heater voltage was decreased by 1–3 V in subsequent steps. Temperature data were recorded at each steady state condition until transition from film to nucleate boiling occurred. This procedure enabled the estimation of the minimum heat flux in film boiling (Leidenfrost point). The time interval between consecutive steady state conditions in nucleate boiling was 1–2 h. The corresponding time interval in film boiling was 2–3 h. A typical boiling experiment was 24–30 h in duration. Due to the high evaporation rates in the saturation experiments, the test fluid was replenished periodically (every 8–9 h) to maintain the fluid level at about 5 cm above the silicon wafer surface. This was done well before the next steady state condition was achieved, usually after recording the data for a previous steady state condition. Usually, this was done close to the CHF in the fully developed nucleate boiling region or in the film boiling region. The degassing procedure was not repeated, as the impact of dissolved gases in these regimes is not expected to alter the results significantly.

4 Data Reduction

The mean heat flux in the vertical direction within the copper cylinder was determined as

$$\overline{q''_{\mathrm{Cu}}} = \frac{\sum_{i=1}^{n} \frac{k_{\mathrm{Cu}} \Delta T_i}{\Delta x_i}}{n} \tag{1}$$

where k_{Cu} is the thermal conductivity of copper, and $\Delta T_i / \Delta x_i$ is the axial temperature gradient measured using vertically aligned thermocouples embedded within the copper cylinder. From the energy conservation principle, the mean heat flux on the test wafer was determined using the following relation:

$$\overline{q''_w} = \frac{\overline{q''_{\mathrm{Cu}}}}{A_w} A_{\mathrm{Cu}} \tag{2}$$

Energy conservation was checked by comparing the total power input to the cartridge heaters with the total rate of heat transfer from the boiling surface measured by the thermocouples (Eq. (2)) and was consistent. It should be noted that in the earlier study by Ahn et al. [11] the boiling curve was reported based on $\overline{q''_{\mathrm{Cu}}}$. In this study the boiling curve is reported based on $\overline{q''_w}$, which is a more consistent definition for wall heat flux.

Pool boiling experiments using thin film thermocouples (TFTs) [15] were used to obtain piecewise linear relations (lookup table) for correlating the wall temperature on the silicon surface as a function of the temperature of the copper cylinder. The lookup table was obtained for the surface temperatures in the nucleate boiling and film boiling regimes. The look up table also enabled the revision of the superheat values reported in the earlier study [11]. The uncertainty in estimating the wall temperature from the copper cylinder temperature using the lookup table is ±1°C. The uncertainty in heat flux within the copper cylinder was evaluated using the procedure of Kline and McClintock [16]. The uncertainty in surface temperature estimates on the test wafer could be from a number of sources.

1. The resolution of the data acquisition system was set by the hardware to a 16 bit accuracy, which was equivalent to an absolute error of ±0.005°C for the temperature range in this study.
2. During the experiments in this study, the standard deviation of temperature fluctuations at steady state conditions was measured to be ~±0.05°C.

Hence the total uncertainty of the temperature measurement was estimated to be ±0.055°C. Using the uncertainty values of ±1.0% for thermal conductivity for copper and of ±3.0% (machining accuracy) for the distance between two thermocouples embedded in the copper cylinder, the estimated maximum uncer-

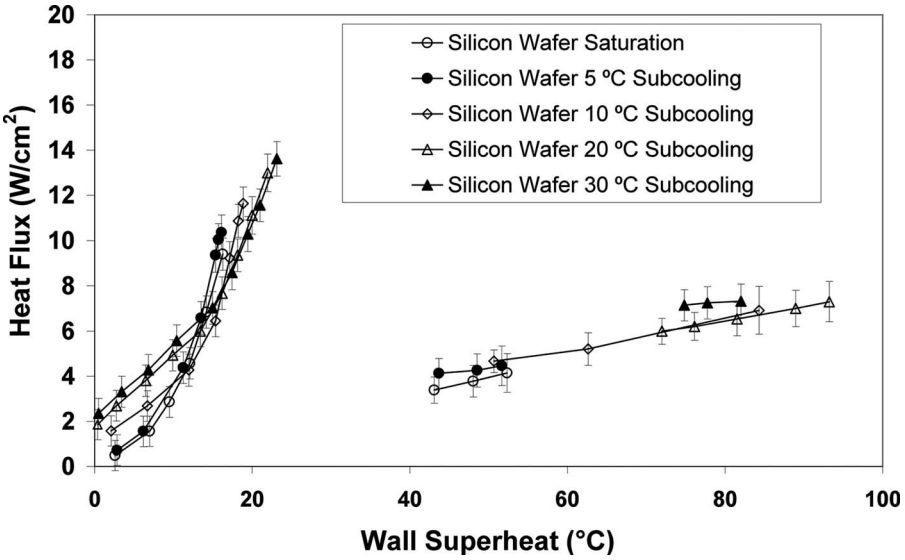

Fig. 2 Pool boiling curves for bare silicon surface at different values of liquid subcooling in nucleate and film boiling regimes

tainty of the surface heat flux near the Leidenfrost (minimum heat flux (MHF)) point was ±14%. The uncertainty was estimated to be ±6% near the CHF point.

5 Experimental Results

The pool boiling heat fluxes for the nanostructured surfaces were compared with the heat flux for an atomically smooth bare silicon wafer surface (this served as the control experiment). The experiments were repeated at least twice to ensure repeatability. An atomically smooth bare surface was chosen for the substrates as well as for the control experiments.

The rationale behind choosing silicon as a substrate was to isolate the effect of nanotubes from that of nucleating cavities on the pool boiling heat transfer rates. Variation in the number of active nucleating cavities can result in higher heat fluxes especially in the low heat flux regime. The random and nonuniform distribution of nucleating cavities that are typically encountered on commercial surfaces (e.g., copper) are difficult to characterize, and there is little control over this experimental variable for different substrates of the same material. The aim of the study was to study the effect of liquid subcooling exclusively on the efficacy of the nanostructured surfaces for enhancing heat transfer. Hence, the transport mechanisms on the nanostructures needed to be decoupled from the interferences due to random effects (i.e., random and uncontrolled distribution of nucleating cavities on the substrate). Heat fluxes in these experiments were substantially lower than those observed in commercial surfaces. Additionally, the carbon nanotubes used in this study were 9–25 μm in thickness and 8–16 nm in diameter. At these length-scales (nanometers to microns), a random uncontrolled variable such as cavity distribution can affect the interpretation of the experimental data significantly. Therefore, atomically smooth substrates were chosen for coating with carbon nanotubes.

5.1 Effect of Subcooling on Bare Silicon Surface. Control experiments performed with a bare silicon wafer provided the base line data for comparison with the heat flux data for MWCNT surfaces. The control experiments served to identify the dominant mechanisms for heat flux enhancement. Boiling inception was obtained by increasing power input to cartridge heaters. Liquid subcooling of 5°C, 10°C, 20°C, and 30°C were maintained using a copper coiled tube heat exchanger. Figure 2 shows the experimental results for a representative run on the bare silicon wafer for saturated and subcooled pool boiling.

In nucleate boiling, the heat flux increases marginally as the liquid subcooling is increased. The CHF points are obtained at wall superheats of 16.3°C, 16.1°C, 18.6°C, 21.9°C, and 23.1°C while the associated heat fluxes are 9.4 W/cm^2, 10.4 W/cm^2, 11.6 W/cm^2, 13.0 W/cm^2, and 13.6 W/cm^2 at saturation, 5°C, 10°C, 20°C, and 30°C subcooling levels, respectively. Ghiu and Joshi [17] conducted pool boiling studies on plain and enhanced copper surfaces with PF-5060 as the working fluid. The studies were carried out at saturation conditions and were restricted to the nucleate boiling regime for wall superheat values less than 29°C. In that study, the plain copper surface showed a maximum heat flux of 15.4 W/cm^2. The enhanced copper surfaces used in Ref. [17] resulted in peak transfer values from 28.9–43 W/cm^2 for different channel widths and pitch.

In the present study, it is observed that at low subcooling (5°C) the boiling curve shifts to the left compared with the saturated boiling curve. This shows that the nucleate boiling heat transfer coefficient increases with subcooling at low wall superheat. However, at high subcooling (10°C and higher) the boiling curve shifts to the right showing that there is a marginal decrease in the nucleate boiling heat transfer coefficient. This behavior is a significant departure from pool boiling curves obtained for commercial surfaces (e.g., copper) [1,2]. Stable film boiling was obtained by decreasing the power input to the heaters immediately after a rapid increase in wall temperature was detected beyond the CHF point. In film boiling, the heat flux increases marginally with subcooling for the low subcooling case of 5°C. There is a significant increase in the wall heat flux at a given wall superheat for higher liquid subcooling. The experimental results show that the Leidenfrost points shift toward higher wall superheat with an increase in subcooling. The Leidenfrost points are obtained at wall superheat of 43.1°C, 43.7°C, 50.7°C, 72°C, and 74.8°C, while the associated wall heat flux values are 3.4 W/cm^2, 4.1 W/cm^2, 4.7 W/cm^2, 6.0 W/cm^2, and 7.1 W/cm^2 for saturated, 5°C, 10°C, 20°C, and 30°C subcooled conditions, respectively.

5.2 Effect of Subcooling on Type-A MWCNT Array (9 μm Tall). Experiments for Type-A MWCNT (9 μm tall) were conducted for subcooling levels of 0–30°C. Figure 3 shows the experimental results for a representative run on the Type-A MWCNT coated wafer for saturated and subcooled pool boiling. Peak heat fluxes increased marginally with an increase in subcool-

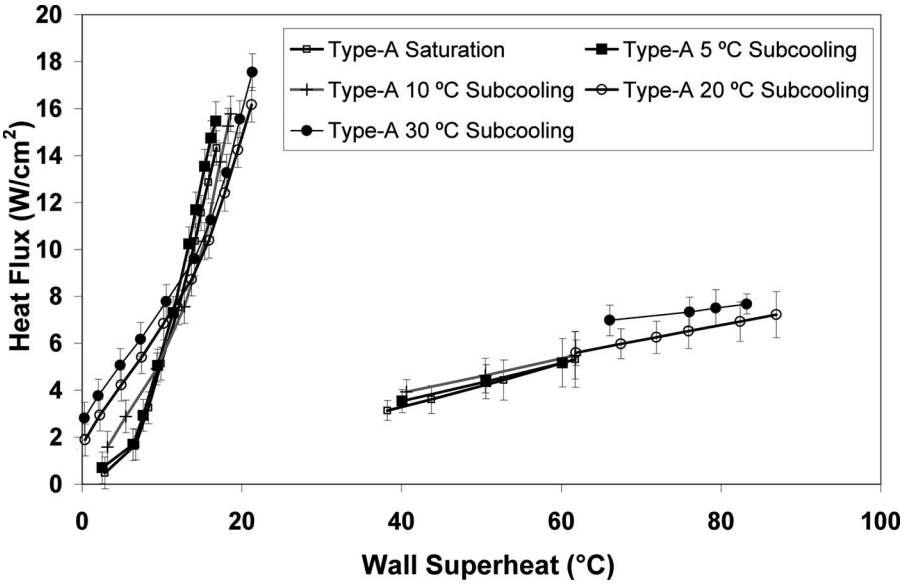

Fig. 3 Pool boiling curves for silicon surface with Type-A (9 μm tall) MWCNT, for different values of liquid subcooling in nucleate and film boiling regimes

ing. This is in contrast to the significant enhancement in heat flux observed for similar conditions on the bare silicon wafer. For liquid subcooling of 10°C, as shown in Fig. 5, the CHF condition was achieved at a higher wall superheat than 5°C subcooled and saturated conditions. Under 5°C subcooling, the CHF point was obtained at the wall superheat of 16.7°C and the associated heat flux was 15.5 W/cm^2. For the saturated condition, the wall superheat at the CHF and the associated heat flux were 16.8°C and 14.3 W/cm^2, respectively. At 20°C subcooling, peak heat flux values near the CHF was 16.2 W/cm^2 at a wall superheat of 21.2°C. It is observed that at low subcooling (5°C) the boiling curve shifts to the left compared with the saturated boiling curve. Thus, the effect of subcooling on the heat transfer coefficients for Type-A MWCNT was the same as that for a bare silicon wafer. Similar variations in heat transfer coefficients at low wall superheat were observed at low (increase in heat transfer coefficients) and high (decrease in heat transfer coefficients) levels of subcooling. In film boiling, marginal enhancements in wall heat flux values were observed as the liquid subcooling was increased for the low subcooling cases within the limits of experimental uncertainty. The Leidenfrost point was achieved at higher wall superheat as the liquid subcooling increased. A similar trend was observed for the pool boiling on silicon wafer.

5.3 Experiments Using Type-B MWCNT array (25 μm Tall). Experiments for Type-B MWCNT (25 μm tall) were conducted for subcooling levels of 0–30°C. Figure 4 shows the experimental results for a representative run on the Type-B MWCNT coated wafer for saturated and subcooled pool boiling. At 10°C subcooling, the wall heat flux near the CHF was 18.4 W/cm^2 at a wall superheat of 21.4°C. The CHF values at 5°C subcooling and saturated conditions were 16.8 W/cm^2 at a

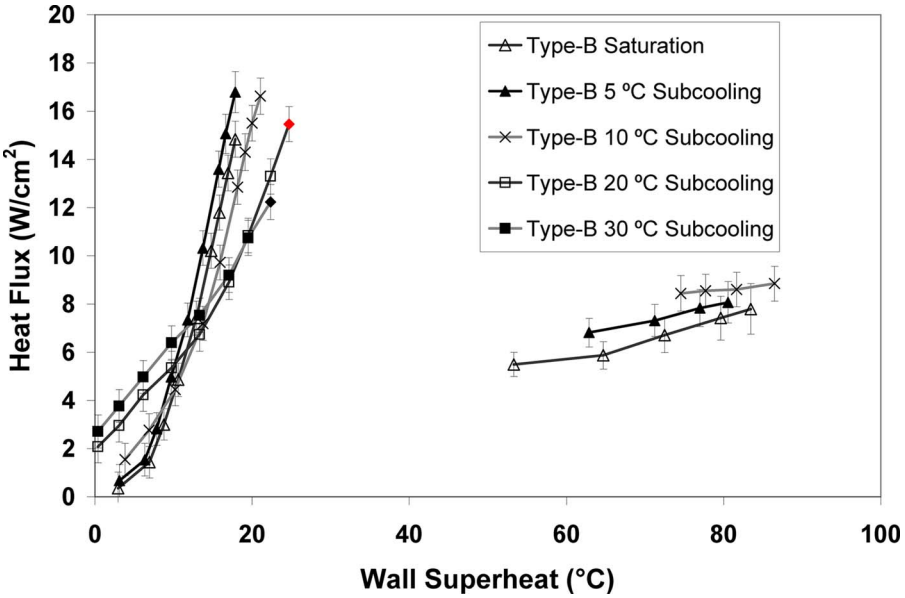

Fig. 4 Pool boiling curves for boiling on silicon surface with Type-B (25 μm tall) MWCNT, for different values of liquid subcooling in nucleate and film boiling regimes

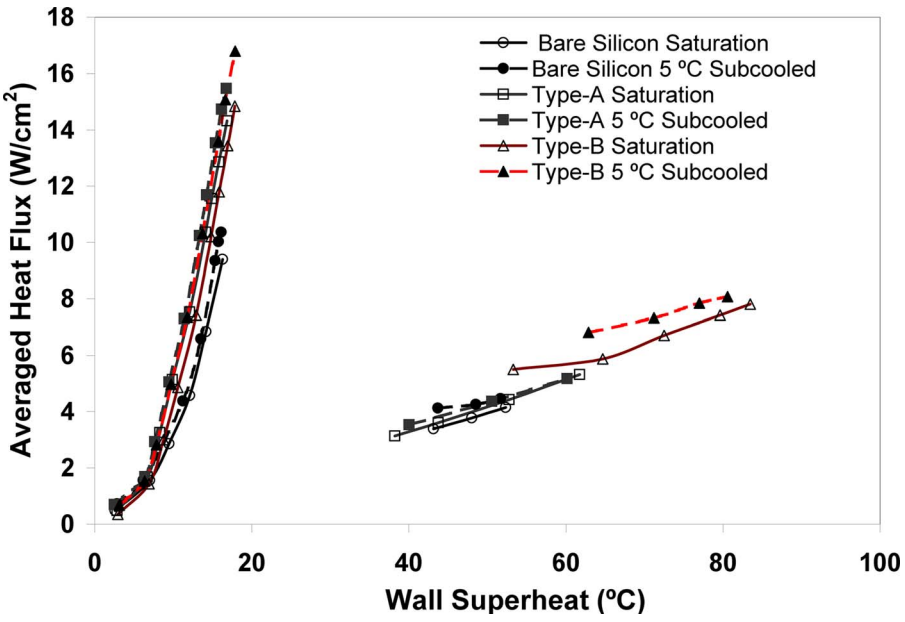

Fig. 5 Pool boiling curves for different surfaces at low values of liquid subcooling

wall superheat of 17.9°C. The CHF condition could not be sustained at 20°C and 30°C subcooling levels due to the limitations of the experimental apparatus. In these experiments before the CHF condition could be attained, the temperature within the copper cylinder exceeded 250°C—which is the maximum temperature rating for the cartridge heaters. Therefore the experiments were terminated. Hence the CHF condition and film boiling data could not be obtained for Type-B MWCNT for liquid subcooling of 20°C and 30°C. The peak heat flux values obtained in these cases are marked with a different symbol in Fig. 5. The nucleate boiling results reported in Fig. 5 are the maximum attained heat flux with the experimental apparatus used in this study.

For Type-B MWCNT, the extent of the wall superheat for the transition boiling region was much larger and more distinct than that for the bare silicon and Type-A MWCNT surfaces. This was due to significant disruption of the vapor film by the nanotubes. During transition from nucleate to film boiling, the film began forming at the edges of the test section and later spread to the center of the test section. At a wall superheat of 53.3°C under saturated boiling condition, a continuous vapor film was observed over the whole area of the exposed surface. The heat flux at the Leidenfrost point was enhanced by as much as ~150% (2.5 times) in film boiling for Type-B MWCNT compared with that for bare silicon wafer (and Type-A MWCNT).

As the liquid subcooling increased, the Leidenfrost point was observed at higher wall superheats. This was consistent with observations for the bare silicon surface (and Type-A MWCNT). The MHF points for Type-B MWCNT occurred at wall superheats of 53.3°C, 62.9°C, and 74.6°C with heat transfer rates of 5.5 W/cm^2, 6.8 W/cm^2, and 8.4 W/cm^2, respectively, under saturated, 5°C subcooled, and 10°C subcooled conditions, respectively. These heat transfer rates were substantially higher (66–150%) than corresponding values obtained for the bare silicon surface under same subcooling conditions.

5.4 Comparison of Type-A MWCNT, Type-B MWCNT, and Bare Silicon. Images of pool boiling on the bare silicon wafer, and Type-A, and Type-B MWCNT surfaces were acquired during the tests. Images were captured during the experiments in proximity to the CHF and the MHF points using a Sony Cyber-Shot DSC-P10 Digital Camera and a Canon® S3IS camera (for subcooling cases of 20°C and 30°C) under saturated and subcooled (5°C, 10°C, 20°C, and 30°C) liquid conditions. In the vicinity of the CHF points, the degree of liquid subcooling strongly influenced the bubble nucleation density, growth, and departure process. Under 10°C subcooling, no bubble columns were observed in vicinity of the CHF point probably because of the condensation effect of the subcooled liquid on the departing bubbles. In contrast, bubble columns were noticeable at the CHF for saturated pool boiling. Relatively weak bubble columns were observed for 5°C subcooled condition. A large number of small bubbles were observed to depart at high subcooling conditions close to the CHF point. By comparing the images taken under the saturated conditions, it was observed that Type-A and Type-B MWCNT surfaces displayed much more ebullient motion of the bubble columns (departing bubbles were larger in size), than for the bare silicon wafer. However, the motion of the departing bubbles during nucleate boiling for the two nanotube coated substrates (Type-A and Type-B MWCNTs) and the bare silicon surface were similar as the liquid subcooling increased. Furthermore, in all cases the MWCNT coated wafers showed a significantly larger number of bubbles departing per unit area of the wafer than the silicon wafer. Thus, the MWCNT coated wafers were observed to have higher nucleation site densities.

The degree of liquid subcooling strongly affected the shape of the departing bubbles and the texture of the stratified vapor film in the vicinity of the Leidenfrost point as it did in the proximity of the CHF point. As the liquid subcooling increased, the amount of vapor bubbles released and the size of bubbles departing from the surface decreased. For all the images, under saturation condition in the vicinity of the Leidenfrost point, a thin film was clearly observed on top of the test surface in the form of a shiny "mirror" type surface. The vapor film had a wrinkled appearance under saturation and low subcooling conditions due to "turbulent" film boiling [18]. In contrast, the subcooled cases showed a relatively smooth "laminar" film boiling. In this study, the vapor film had a wrinkled appearance under saturation and low subcooling conditions. At high subcooling levels, the vapor film had a less wrinkled appearance.

In nucleate boiling, both Type-A and Type-B MWCNT surface had higher wall heat flux values than the corresponding values for the bare silicon surface under saturated and subcooled conditions (5°C and 10°C), as shown in Figs. 5 and 6. For instance, at a given wall superheat of 10°C and under saturation condition, Type-A and Type-B MWCNT surfaces, respectively, showed

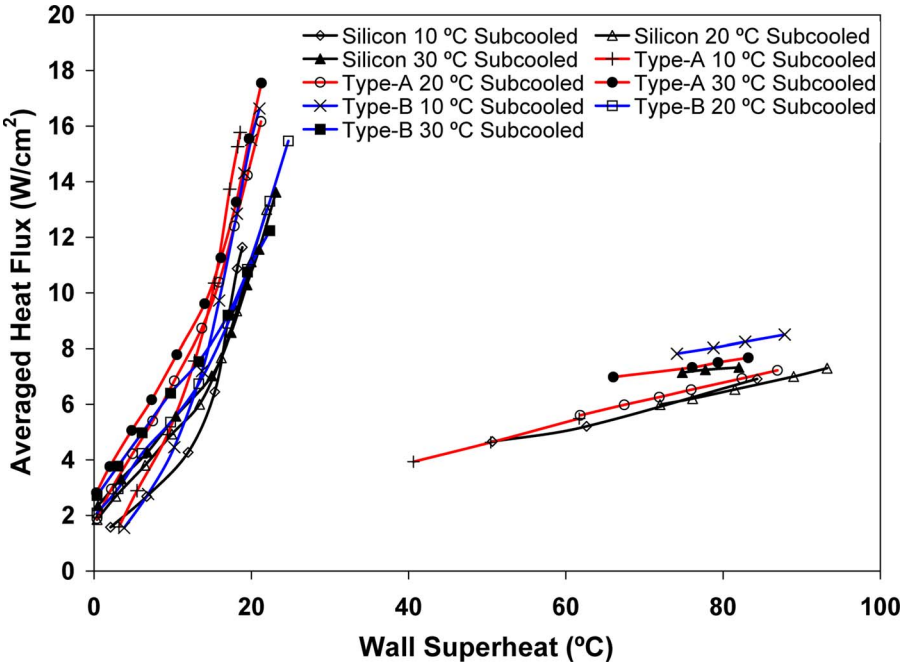

Fig. 6 Pool boiling curves for different surfaces at high values of liquid subcooling

64.6% and 33.0% higher heat fluxes than the bare silicon surface. The wall heat flux values at the CHF for Type-A and Type-B MWCNT surfaces were higher than corresponding values for the bare silicon surface under all of the liquid conditions.

For film boiling experiments under saturated and subcooled (5°C and 10°C) conditions, the wall heat fluxes for Type-B MWCNT were much higher than the corresponding values for Type-A MWCNT and the bare silicon surface. The taller MWCNT (Type-B MWCNT) structures enhanced the wall heat flux at a given wall superheat and caused the MHF point to be attained at higher wall superheat by disrupting the vapor film at the points of minimum vapor film thickness that may lead to possible collapse of the vapor film in film boiling [11,19–21]. Within the bounds of experimental uncertainty, the wall heat flux for Type-A MWCNT matched the corresponding values for the bare silicon wafer at a given superheat. Under saturated and 10°C subcooled conditions, the wall heat flux values for Type-A MWCNT were obtained as 3.1 W/cm^2 and 3.9 W/cm^2, respectively, at wall superheats of 38.2°C and 40.6°C. These were 7% and 15% lower than the corresponding values for the bare silicon wafer under the same liquid subcooling conditions.

As shown in Figs. 5 and 6, the Leidenfrost point for Type-A MWCNT was observed at a slightly lower wall superheat for saturated and subcooled conditions, compared with the bare silicon surface for the low subcooling cases. Also, at low subcooling (5°C), the Leidenfrost point shifted to lower wall superheat for bare silicon and Type-A MWCNT. The wall heat flux values in vicinity of the CHF and the MHF points are summarized in Table 1.

Figure 7 provides a schematic showing the potential disruption of the vapor film by Type-B MWCNT while Type-A MWCNT is not able to disrupt the vapor film. Hence the heat flux from Type-A MWCNT matches that of the bare silicon surface (within the bounds of measurement uncertainty), while Type-B MWCNT results in higher wall heat flux. Further explanation is provided in Sec. 5.

The effect of Type-A MWCNT array on the wall heat flux is compared with that of Type-B MWCNT array and bare silicon wafer in Figs. 6 and 7 for low and high subcooling levels, respectively. In nucleate boiling, under saturated condition, the wall heat flux values for Type-A MWCNT were higher than the corresponding values for Type-B MWCNT under fully developed nucleate boiling conditions. In the fully developed nucleate boiling region, Type-A MWCNT yielded much higher wall heat flux values than the corresponding values for the bare silicon wafer at a given wall superheat. For the saturated condition, the wall superheat at the CHF point and the associated heat flux were 16.8°C and 14.3 W/cm^2, respectively, for Type-A MWCNT. This wall heat flux value was 52.5% higher than the corresponding CHF value for the bare silicon surface. Type-B MWCNT had higher CHF values under saturated and 5°C subcooled conditions, respectively, than Type-A MWCNT. The associated wall superheat values for Type-B MWCNT were also slightly higher than the corresponding values for Type-A MWCNT under both saturated and 5°C subcooled conditions. Under 5°C subcooled conditions, Type-A MWCNT enhanced heat flux near the CHF by 49.3% compared with the bare silicon wafer (control experiment). The CHF values for Type-B MWCNT under saturated and 10°C subcooled conditions were 58% higher for the former and 19–58% higher for the latter when compared with corresponding values for the bare silicon wafer at same level of subcooling.

6 Discussion

The effect of MWCNT on pool boiling can be summarized to be due to the following.

1. The higher "effective" wall thermal conductivity due to the presence of MWCNT, which can enhance the spatial size of the wall temperature fluctuations or "cold-spots."
2. The thickness of the "hairlike" MWCNT vertical protrusions (which can disrupt the hydrodynamic instabilities, e.g., by disrupting the microlayer region in nucleate boiling and the "continuous" vapor film in film boiling). This can also lead to enhanced transient heat transfer (compared with bare silicon surface) by increasing the frequency and magnitude of the cyclical liquid-solid contacts.

The experimental results are consistent with numerical models reported in the literature. Previous numerical and experimental results by Banerjee and Dhir [19,20] and Banerjee et al. [21] have shown that the dynamic value of the minimum vapor film thickness for film boiling of PF-5060 is approximately 15–20 μm.

Table 1 Comparison of CHF and MHF values from the pool boiling experiments

Substrate	Bulk liquid subcooling (°C)	CHF		MHF	
		T_{sup} (°C)	Q(W/cm^2)	T_{sup} (°C)	Q(W/cm^2)
	Saturated	16.3	9.4	43.1	3.4
	5	16.1	10.4	43.7	4.1
	10	18.9	11.6	50.7	4.7
	20	21.9	13.0	72.0	6.0
	30	23.1	13.6	74.8	7.1
Bare					
	Saturated	16.8	14.3	38.2	3.1
	5	16.7	15.5	40.0	3.5
	10	18.6	15.8	40.6	3.9
	20	21.2	16.2	61.8	5.6
	30	21.3	17.5	66.0	7.0
Type-A					
	Saturated	17.8	14.8	53.3	5.5
	5	17.9	16.8	62.9	6.8
	10	21.4	18.4	74.6	8.4
	20	(24.7)[a]	(15.5)[a]	-	-
Type-B	30	(22.4)[a]	(12.2)[a]	-	-

[a]The maximum values obtained from the experiments are reported since critical heat flux condition could not be attained in the experiments.

The authors had discussed that surface roughness (or for example artificially engineered surface micro/nanostructures) greater than 20 μm could disrupt the vapor films at the points of minimum vapor film thickness leading to possible collapse of film boiling.

Comparing the results of Type-A and Type-B MWCNT surface, it is observed that for Type-B (25 μm tall) the film boiling is enhanced considerably more than for Type-A (9 μm thickness). This shows that an MWCNT surface with thickness greater than 20 μm possibly disrupts the vapor film. Therefore, MWCNT surface with thickness greater than 20 μm have better efficacy in enhancing heat transfer in film boiling. The effect of subcooling on heat flux enhancement is therefore more pronounced for Type-B MWCNT than for Type-A MWCNT. This mechanism is schematically demonstrated in Fig. 1.

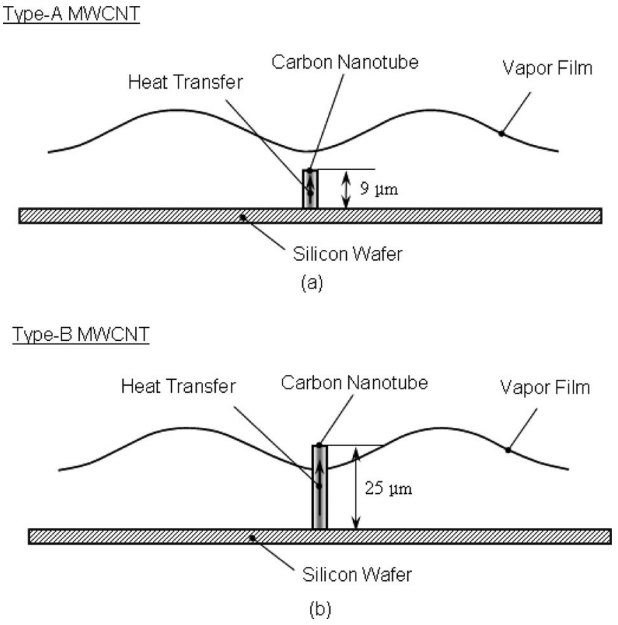

Fig. 7 Schematic of the heat transfer mechanism for carbon nanotubes in film boiling: (*a*) Type-A (9 μm thickness), and (*b*) Type-B (25 μm thickness) MWCNT

The study of Banerjee et al. [19–21] also demonstrated the existence of cold-spots in film boiling. Cold-spots are regions of lower surface temperature than the surrounding. The study by Banerjee et al. [19–21] showed that cold-spots serve as focused conduits for heat transfer in film boiling. The location of the cold-spots coincided with the location of the minimum vapor film thickness (showing that these are coupled thermal-hydrodynamic phenomena). The width of the cold-spots was a function of the wall thermal conductivity (or more specifically the thermal diffusivity of the wall material). It is expected that similar "cold spot" regions develop during nucleate boiling in the "microlayer region" on the wall. By analogy, it would be expected that the size (or width) of the cold-spots under the microlayer would be dictated by the wall thermophysical properties.

Since MWCNT structures have higher thermal conductivity than the silicon substrate, the size of the cold-spots is bigger for surfaces coated with MWCNT than for the bare silicon wafer. Hence the efficacy of the cold-spots is enhanced due to the presence of the MWCNT structures. MWCNT structures that disrupt the vapor film at the minimum vapor film thickness (or location of the cold-spots) would enhance the liquid-solid contacts and cause transient quenching of the heater surface with further augmentation of heat transfer in film boiling. Hence, Type-B MWCNT surface causes heat transfer augmentation in film boiling while heat transfer augmentation is not observed during the film boiling experiments for Type-A MWCNT surface.

From Fig. 5 it is observed that there is marginal enhancement in film boiling heat transfer (~20%) at a liquid subcooling of 5°C for the bare silicon wafer. At liquid subcoolings of 10°C, 20°C, and 30°C, the film boiling heat fluxes are enhanced by ~25%, ~80%, and ~125%, respectively, for both bare silicon and Type-A MWCNT. The heat flux is marginally higher for Type-A MWCNT than for bare silicon in the film boiling regime at subcooling of 30°C and is similar to the heat flux values for Type-B MWCNT in subcooled film boiling at low levels of subcooling, within the bounds of the measurement uncertainty. This is consistent with numerical predictions in the literature. Numerical studies reported by Banerjee and Dhir [19,20] show that the minimum value of the dynamic vapor film thickness decreases with an increase in subcooling. Banerjee and Dhir [19,20] predicted that for subcooling of 10°C the minimum vapor film thickness is greater than 15 μm for film boiling. Hence, at subcooling greater than

10°C vapor film thickness is expected to be lower than 15 μm. The experimental results show that at subcooling exceeding 10°C, the heat flux is enhanced by 80–115%, possibly due to a decrease in the minimum thickness of the dynamic vapor film and consequently by the spontaneous disruption of the vapor film (similar to Fig. 7) by the MWCNT.

In contrast, there is low sensitivity of heat transfer augmentation to the thickness of the MWCNT surface in nucleate boiling. For a wall superheat of 10°C at high subcooling levels of 20°C and 30°C, heat fluxes are enhanced for Type-A MWCNT by 35.8% and 36.9%, respectively, and for Type-B by 10.1% and 14%, respectively, compared with the bare silicon wafer at the same levels of subcooling.

This shows that the enhancement in CHF decreased for the MWCNT coated surfaces with an increase in subcooling (when compared with the corresponding heat flux values on the bare silicon substrate). This is potentially due to the different configurations of vapor column formation at CHF for the nanotube coated surfaces compared with the bare surface (as described above). At low subcooling and saturated pool boiling the bubble size was bigger and had bigger vapor columns. Enhanced heat transfer through the microlayer potentially contributed to the higher bubble departure frequency. However, at higher subcooling, the bubble departure process was similar for nanostructured surfaces and smooth (bare) surfaces. The reason for higher heat flux at high subcooling for the nanotube coated surfaces is potentially due to the higher nucleation site densities.

This is because in nucleate boiling and at the CHF, the size and distribution of the nucleation sites is expected to be the limiting variable rather than the thickness of the surface structures. The thickness of the MWCNT in these experiments is greater than the thickness of the microlayer [2]. The thickness of the microlayer is estimated to be in the range of 10–100 nm [1,2]. Therefore, both types of MWCNT are able to disrupt the microlayer resulting in enhanced liquid-solid contact and, consequently, enabling similar heat flux enhancements at comparable wall superheat values at low subcooling levels. Alternately, the thickness of the microlayer can also be enhanced by capillary wicking due to the presence of the MWCNT "forests" which are 8–16 nm in diameter and of comparable pitch. Such a high spatial density of hairlike protrusion can provide enough capillary pressure to increase the thickness of the microlayer (estimated to be by as much as 100%) and therefore provide additional surface area for heat transfer. Hence the interfacial thermal resistance (or Kapitza resistance [2]) can be significantly reduced due to the presence of the MWCNT.

A potential mechanism for the delayed occurrence of CHF at higher superheats could be through the suppression of "mushroom" type of bubbles or enhanced formation of vapor stems that trap superheated liquids at CHF (e.g., Ref. [22]). This can occur due to the hair-like protrusion of the MWCNT into the mushroom type bubble or through formation of additional vapor stems due to presence of MWCNT on the surface. Also, an anomalous behavior is noted at low subcooling where the CHF is enhanced and occurs at lower wall superheat. This is in contrast to the behavior at high subcooling where the CHF is measured to be enhanced and to occur at high wall superheats. This behavior recurred for both nanotube coated surfaces and the MWCNT coated surfaces. Additional investigations are needed to conclusively verify the mechanisms responsible for extending the wall superheat required for CHF for boiling on nanostructured surfaces and to understand the effect of the thickness of the nanostructures on CHF.

7 Conclusions

Boiling experiments were conducted using PF-5060 as the test fluid on silicon wafer substrates. The experiments were conducted with a bare silicon wafer and two silicon wafers containing a uniform layer of vertically aligned MWCNT of two different thicknesses, respectively (Type-A: 9 μm and Type-B: 25 μm).

(1) In the nucleate boiling regime, the enhancement heat flux is weakly dependent on the thickness of the MWCNT.
(2) The heat flux enhancement for nanotube coated substrates decreases with an increase in subcooling. This is potentially due to a change in the morphology of the bubble departure process with an increase in subcooling.
(3) The nucleation site density increases on the nanotube coated surfaces compared with the bare substrate.
(4) In nucleate boiling, MWCNT coated substrates (both 9 μm and 25 μm thickness) yield higher wall heat fluxes under saturated and subcooled conditions compared with a bare silicon surface. The Type-B MWCNT array augments CHF by ~62% compared with a bare silicon surface under saturated and 10°C subcooling, respectively.
5) Wall heat flux values near the CHF for Type-B MWCNT exceed those for Type-A MWCNT under saturated condition.
(6) In the film boiling regime, the heat flux is sensitive to the thickness of the MWCNT coating. For Type-B MWCNT (25 μm thickness) the wall heat flux values are enhanced under saturated (~62%), 5°C subcooling (~62–124%), 10°C subcooling conditions (~66–148%), compared with control experiments performed on a bare silicon surface. However, for Type-A MWCNT (9 μm thickness) the wall heat flux values are similar to the corresponding values for the bare silicon surface during film boiling, for low subcooling. At high subcooling, the film boiling heat flux values are enhanced significantly and by similar magnitudes for both bare silicon and Type-A MWCNT coated heaters. This is consistent with the dynamic models for film boiling reported in the literature.
(7) Type-B MWCNT coated substrate is more sensitive to subcooling compared with Type-A MWCNT and a bare silicon wafer in the film boiling regime.

Acknowledgment

The authors gratefully acknowledge the support for this study from the Texas Engineering Experimentation Station (TEES), and the Mechanical Engineering Department new faculty startup grant that was awarded in January 2005. The authors gratefully acknowledge the help of Dr. Ray Baughman, Dr. M. Zhang, and Dr. S. Fang, at University of Texas at Dallas, for their help in synthesizing the MWCNT. The authors acknowledge the help of Mr. S. Shriraman (Graduate Student, Texas A&M University) for his help with obtaining the contact angle measurements. The authors also acknowledge the help of Mr. J. Howson, Dr. A. Mukhopadhyay, and Dr. A Bhasin from the Texas Transportation Institute at Texas A&M University for their help with training and accessing the goniometer instrument. Work was performed, in part, at the Microelectronics Research Center at UT Austin of National Nanofabrication Infrastructure Network supported by National Science Foundation under Award No. 0335765.

During this study, V.S., H-S.A., and D.B. were partially supported through various other research programs: National Science Foundation (CBET Grant No. 0630703), seedling grant from Defense Advanced Project Agency (DARPA-MTO), Micro/Nano-Fluidics Fundamental Focus Center (DARPA-MF3) through the University of California at Irvine, New Investigations Program (NIP 2005) of the Texas Space Grants Consortium (TSGC), Office of Naval Research (ONR), Air Force Office of Scientific Research (AFOSR) through the American Society for Engineering Education (ASEE) Summer Faculty Fellowship (SFFP) Program at the Air Force Research Laboratory (AFRL), Army Research Office (ARO) SBIR Phase II subcontract through Lynntech Inc., and the National Science Foundation (NSF) SBIR Phase I through NanoMEMS Research LLC.

Nomenclature

A = area (m^2)
g = acceleration due to gravity (m/s^2)
k = thermal conductivity ($W/m\,K$)
n = total number of pairs of vertically aligned thermocouples
q = average wall heat transfer in the axial direction (W)
$\overline{q''}$ = mean heat flux (W/m^2)
T = temperature (°C)
ΔT_i = temperature gradient between two vertically aligned thermocouples (°C)
ΔT = temperature gradient between top of the copper cylinder and the test surface (°C)
Δx_i = distance between the two vertically aligned thermocouples (m)
ω = relative uncertainty

Subscripts

Cu = copper cylinder
j, k = thermocouple position in a vertically aligned plane
sat = saturation condition
sup = wall superheat
v = vapor property
w = wall (boiling surface)

References

[1] Dhir, V. K., 1998, "Boiling Heat Transfer," Annu. Rev. Fluid Mech., **30**, pp. 365–401.
[2] Carey, V. P., 1992, *Liquid-Vapor Phase-Change Phenomena*, Taylor & Francis, London.
[3] Ramaswamy, C., Joshi, Y. K., Nakayama, W., and Johnson, W. B., 2000, "Combined Effects of Subcooling and Operating Pressure on the Performance of a Thermo-Siphon," IEEE Trans. Compon. Packag. Technol., **23**(1), pp. 61–69.
[4] Ramaswamy, C., Joshi, Y., Nakayama, W., and Johnson, W. B., 2003, "Effects of Varying Geometrical Parameters on Boiling From Microfabricated Enhanced Structures," ASME J. Heat Transfer, **125**, pp. 103–109.
[5] Mudawar, I., and Anderson, T. M., 1993, "Optimization of Enhanced Surfaces for High Flux Chip Cooling," J. Electron. Packag., **115**, pp. 89–100.
[6] Coursey, J., Roh, H. K., Kim, J. H., and Boudreaux, P. J., 2002, "Graphite Foam Thermosyphon Evaporator Performance," *Proceedings of the ASME IMECE2002*, New Orleans.
[7] Iijima, S., 1991, "Helical Microtubules of Graphitic Carbon," Nature (London), **354**, pp. 56–58.
[8] Berber, S., Kwon, Y. K., and Tomanek, D., 2000, "Unusually High Thermal Conductivity of Carbon Nanotubes," Phys. Rev. Lett., **84**, pp. 4613–4616.
[9] Ujereh, S., Mudawar, I., Amama, P. B., Fisher, T., and Qu, W., 2005, "Enhanced Pool Boiling Using Carbon Nanotube Surface on a Silicon Surface," ASME Paper No. IMECE2005-80065.
[10] Ujereh, S., Fisher, T., and Mudawar, I., 2007, "Effects of Carbon Nanotube Arrays on Nucleate Pool Boiling," Int. J. Heat Mass Transfer, **50**(19-20), pp. 4023–4038.
[11] Ahn, H.-S., Sinha, N., Banerjee, D., Zhang, M., Feng, S., and Baughman, R., 2006, "Pool Boiling Experiments on Multi-Walled Carbon Nanotube Forests (MWCNT)," ASME J. Heat Transfer, **128**, pp. 1335–1342.
[12] Zhang, M., Atkinson, K. R., and Baughman, R., 2004, "Multifunctional Carbon Nanotube Yarns by Downsizing an Ancient Technology," Science, **306**, pp. 1358–1361.
[13] Zhou, J. J., Noca, F., and Gharib, M., 2006, "Flow Conveying and Diagnosis With Carbon Nanotube Arrays," Nanotechnology, **17**, pp. 4845–4853.
[14] Bhavnani, S., Fournelle, G., and Jaeger, R. C., 2000, "Immersion-Cooled Heat Sinks for Electronics: Insight From High-Speed Photography," *Proceedings of the Seventh Intersociety Conference on Thermal and Thermomechanical Phenomena in Electronic Systems*, Vol. 2, pp. 310–311.
[15] Ahn, H. S., Sathyamurthi, V., Sinha, N., Lau, S., and Banerjee, D., 2005, "Boiling Experiments on Vertically Aligned Carbon Nanotubes and Using Surface Micromachined Thin Film Thermocouple (TFT)," *Proceedings of the Ninth AIAA/ASME Thermophysics and Heat Transfer Conference*, San Francisco, CA, June 5–8.
[16] Kline, S. J., and McClintock, F. A., 1953, "Describing Uncertainties in Single-Sample Experiments," Mech. Eng. (Am. Soc. Mech. Eng.), **75**, pp. 3–8.
[17] Ghiu, C.-D., and Joshi, Y., 2005, "Boiling Performance of Single-Layered Enhanced Structures," ASME J. Heat Transfer, **127**, pp. 675–683.
[18] Chang, Y. P., 1959, "Wave Theory of Heat Transfer in Film Boiling," ASME J. Heat Transfer, **81**, pp. 1–12.
[19] Banerjee, D., and Dhir, V. K., 2001, "Study of Subcooled Film Boiling on a Horizontal Disc: Part 1 Analysis," ASME J. Heat Transfer, **123**, pp. 271–284.
[20] Banerjee, D., and Dhir, V. K., 2001, "Study of Subcooled Film Boiling on a Horizontal Disc: Part 2 Experiments," ASME J. Heat Transfer, **123**, pp. 285–293.
[21] Banerjee, D., Son, G., and Dhir, V. K., 1996, "Conjugate Thermal and Hydrodynamic Analysis of Saturated Film Boiling From a Horizontal Surface," ASME HTD **334** (Part 3), pp. 57–64.
[22] Gaertner, R. F., 1963, "Distribution of Active Sites in the Nucleate Boiling of Liquids," Chemical Engineering Progress Symposium Series, Vol. 59, pp. 52–61.